Corrosion Science xxx (2017) xxx-xxx

Contents lists available at ScienceDirect

Corrosion Science

journal homepage: www.elsevier.com

Effect of brief thermal aging on stress corrosion cracking susceptibility of LDSS 2101 in the presence of chloride and thiosulphate ions

F. Zanotto[a,*], V. Grassi[b], A. Balbo[b], C. Monticelli[b], C. Melandri[c], F. Zucchi[b]

[a] Terra&AcquaTech Laboratory, University of Ferrara, Via Saragat 1, 44122 Ferrara, Italy
[b] Corrosion and Metallurgy Study Centre "Aldo Daccò", University of Ferrara, Via G. Saragat 4A, 44122 Ferrara, Italy
[c] ISTEC-CNR, Via Granarolo 64, 48018 Faenza, Italy

ARTICLE INFO

Keywords:
A. Stainless steel
C. Hydrogen embrittlement
C. Stress corrosion

ABSTRACT

In this paper, the effect of brief aging within the 650–850 °C temperature range on the resistance of lean duplex stainless steel (LDSS) 2101 to stress corrosion cracking (SCC) was discussed. The thermal aging induced a decrease in Vickers microhardness and an increase in alloy ductility. This behaviour was connected to depletion of interstitial nitrogen in austenite. LDSS 2101 was found to suffer SCC in NACE TM-0177 solution, particularly under specific thermal aging and in the presence of thiosulphate ions ($S_2O_3^{2-}$) at 10^{-4} and 10^{-3} M. Crack nucleation and propagation were linked to microstructural variations connected to thermal aging.

1. Introduction

In the last 20 years, the development of austenitic-ferritic stainless steels, more commonly known as duplex stainless steels (DSS), has followed two different paths: the improvement of corrosion performances by increasing chromium, molybdenum and nitrogen content (superduplex and hyperduplex grades) and the developing of the so called "lean" duplex family [1]. The lean duplex stainless steels (LDSSs) were conceived to lower the molybdenum content, which can cause dangerous secondary phase formation during welding operations, and to reduce the nickel content in order to limit raw material costs in duplex production. In 2002, LDX 2101® (a low nickel grade) was commercially introduced with the aim of advantageously replacing austenitic stainless steels (AISI 304 and 316), in applications where high mechanical and localized corrosion resistance are required [2–5], but also, to some extent, to substitute carbon steels, where maintenance costs are significant [1].

The mechanical properties and the corrosion resistance of ordinary DSS can be adversely affected by aging within the 650–950 °C range [6], mainly due to σ phase formation [7–15]. However, in LDSS the growth of this compound is very slow, because of the low molybdenum content [4,16], and may affect the performances of these alloys only after long aging time (on the order of 100 h [4,17]).

LDSS 2101 contains high amounts of manganese (5 mass%) and nitrogen (0.22 mass%) [18] added with the aim to stabilize the austenite phase. The influence of N content is quite complex. In fact, it improves the pitting corrosion resistance and stimulates cracks repassivation [19,20]. It also enhances the mechanical strength, even at low concentrations (i.e. 0.1–0.2%) [21,22]. In DSS, it increases the microhardness of both ferrite (α) and austenite (γ) phase, with a more pronounced effect on γ [22], because this phase can dissolve higher nitrogen amounts. For this reason, in DSS the γ phase becomes the strongest one at N concentrations higher than 0.12 wt.% [23,24]. On the other side, it is reported to reduce the stacking fault energy (SFE) of austenite phase, so promoting planar slip and easier passive film breakdown, when slip/dissolution mechanism is involved in SCC [25,26].

Other problems connected to high nitrogen levels occur after thermal aging because precipitation of nitrides (e.g. Cr_2N) at the grain boundaries occurs already after few minutes of aging in the 650–850 °C interval [27–30]. During a previous research carried out in our laboratory on LDSS 2101 [30], these microstructural modifications are found to determine a worsening of pitting and intergranular corrosion (IGC) resistance. In particular, a very low resistance to pitting corrosion and high values of the degree of sensitization (DOS) to IGC were obtained, particularly after 30 and 60 min of aging at 650 °C and 10 and 30 min at 750 °C. On the contrary, aging at 850 °C for up to 30 min essentially did not modify the resistance to ICG and only slightly decreased that to pitting corrosion, likely due to chromium replenishment around nitride precipitates. Liu et al. [17] documented the structural evolution of LDSS 2101 for thermal aging at 600–850 °C and looked for a connection between variations in mechanical properties

* Corresponding author.
Email address: federica.zanotto@unife.it (F. Zanotto)

https://doi.org/10.1016/j.corsci.2017.10.024
Received 27 June 2017; Received in revised form 3 October 2017; Accepted 20 October 2017
Available online xxx
0010-938/ © 2017.

UNCORRECTED PROOF

and pitting resistance. In agreement with Berner et al. [27], they found a significant reduction of both critical pitting temperature (CPT) and impact toughness after few minutes of aging at 750 °C, which resulted the temperature leading to the most severe degradation of the alloy performances. All quoted studies evidenced that these short-time thermal aging provoked formation of Cr-rich precipitates (mainly Cr_2N but also $M_{23}C_6$-type carbides) at the phase grain boundaries and Cr-depletion in the adjacent zones, determining an easier localization of corrosion attack.

Oil and gas equipment often operate in contact with chloride- and sulphide-rich media. Therefore, the employed materials have to resist to pitting corrosion and stress corrosion cracking (SCC) in these environments. LDSS 2101 has a resistance to pitting and crevice corrosion, which is higher than that of austenitic 304 L and is comparable to that of 316 L [2,5]. Even SCC resistance is superior to that of standard austenitic grades. This makes LDSS 2101 a suitable candidate for oil and gas industry applications, in mild well conditions and topside components [18,31] and the study of its corrosion performances in simulated oil and gas conditions is reputed quite important.

Several works in literature concern the SCC resistance of ordinary DSS 2205 [32–36] or superduplex stainless steels [37–39] in environments containing hydrogen sulphide (H_2S). Few data are reported about the SCC behaviour of lean duplex 2304 and LDSS 2101 in the presence of H_2S [18,40]. In our laboratory, the slow strain rate technique was applied to LDSS 2101 during exposures to 20% NaCl solution at 80 °C and to standard NACE TM-0177 solution at 25 °C, in the presence of thiosulphate ions ($S_2O_3^{2-}$) at various pH and temperatures [40]. In fact, as proposed by Tsujikawa et al. [41,42], it is possible to substitute H_2S with $S_2O_3^{2-}$ ions in laboratory studies aiming to estimate the sulphide SCC susceptibility of alloys in sour environments. The use of $S_2O_3^{2-}$ ions in replacement of H_2S gas can minimize the health hazards in laboratory tests and therefore can reduce the costs to ensure safe working conditions [43]. Our research [40] showed that LDSS 2101 was susceptible to SCC even in the presence of small amounts of $S_2O_3^{2-}$. However, in dependence of $S_2O_3^{2-}$ concentration, pH and temperature of the solution, also a diffuse selective attack of ferrite phase occurred during slow strain rate tests (SSRT). Actually, selective dissolution of ferrite in LDSS 2101 was detected also in the presence of chlorides and H_2S [18] and this behaviour must be taken into account when these alloys are used in oil and gas field.

In the present paper, the influence of brief aging performed between 650 and 850 °C on SCC susceptibility of LDSS 2101 was studied in standard NACE TM-0177 solution at pH 2.7 and 25 °C, in the absence and presence of $S_2O_3^{2-}$ at 10^{-4} and 10^{-3} M.

2. Experimental

Tests were performed on LDX 2101® stainless steel (supplied by Outokumpu Company under annealed conditions) with nominal chemical composition (mass%) reported in Table 1.

Tensile samples with an overall length of 23 cm and a gauge portion of 20 × 5 × 1.5 mm were machined from a 1.5 mm thick steel sheet. The samples were aged at 650 °C for 30 and 60 min and at 750 and 850 °C for 5, 10 and 30 min and then air cooled. The resulting microstructures were observed by Zeiss EVO MA15 scanning electron microscope (SEM) in back-scattered electron (BSE), in order to reveal the presence of secondary phases.

Before and after thermal aging, Vickers microhardness (HV) measurements were carried out to evaluate the alloy hardness, while nanoindentation tests were performed to determine the hardness of the single ferrite and austenite phases. Both tests were carried out on samples ground to 2500 grit emery papers, polished with diamond pastes (from 6 to 1 μm), rinsed with deionized water and finally degreased with acetone. HV values were the average of 5 measurements obtained with an applied load of 10 N. In order to measure the dispersion of each set of HV data, standard deviations were calculated.

Load-controlled nanoindentation tests were performed by employing a commercial nanoindenter (Nanoindenter XP MTS, Oak Ridge, TN, USA) using a Berkovich diamond tip. The peak load was 5 mN. The indenter was continuously loaded up to the peak load and immediately unloaded with no holding time. From each load-displacement curve the maximum contact depth (h_{max}) and the maximum indentation load (P_{max}) parameters were derived, together with the estimated area of contact (A). The latter was determined by Oliver and Pharr method [44], directly from the geometry of the Berkovich indenter and h_{max} (nanoindenter software TestWorks TM ver. 4.06A). The nanoindentation hardness was finally computed as the ratio between the measured P_{max} and the corresponding calculated A. The area function of the indenter tip was calibrated on a standard silica sample for a contact depth range corresponding to those measured on the LDSS samples. A 10 × 4 grid of indentations, horizontally spaced 5 μm and vertically spaced 4 μm, was performed on each sample. After nanoindentation tests, samples were observed with SEM in BSE modality, in order to classify each indentation as located in either ferrite or austenite grains or discharged, due to proximity to an interface boundary. The accepted ferrite and austenite hardness data (expressed in GPa) were separately averaged to obtain the mean hardness values of each phase and data dispersion was quantified by calculating standard deviation.

The susceptibility to SCC was evaluated by SSRT, with a strain rate of 1×10^{-6} s^{-1} [45]. After thermal aging, the samples were ground parallel to the stress direction down to 800 grit emery papers and screened by a two-component epoxy varnish, so leaving only the gauge portion exposed to the solution. SSRT were performed by inserting the sample in an electrochemical cell, which was filled by deaerated 5% NaCl + 0.5% CH_3COOH solution (the basic standard solution NACE TM-0177 [46], without saturated H_2S gas) in the absence and presence of 10^{-4} or 10^{-3} M $Na_2S_2O_3$, at 25 °C and pH 2.7. During each test, the stress – strain curve was recorded. Stress (in MPa) is the ratio of the applied load to cross section area of the gauge portion (5 mm x 1.5 mm) in tensile samples, while strain is the ratio of the elongation of the sample to its original length, as evaluated from the relative movement of the tensile machine crosshead. The obtained strain values are unitless, but they were expressed in percentage, as they were multiplied by 100. In parallel to stress-strain curve recording, corrosion potential (E_{cor}, versus Saturated Calomel Electrode (SCE)) values were measured. Reference SSRT in air at 25 °C were also carried out. Each test was performed in triplicate.

The SCC susceptibility was evaluated by the ratio, R, between the percentage fracture elongation (ε_f%) of samples exposed to the test solution and the corresponding ε_f% in air. At the end of the tests, side surfaces of the samples (sections parallel to load direction in SSRT) were polished and examined by optical stereomicroscope, and by SEM, with the purpose to analyze crack initiation and morphology.

Table 1
Nominal chemical composition (mass%) of LDSS 2101.

Elements	C	Mn	Cr	Ni	Mo	N	Fe
%	0.03	5.0	21.5	1.5	0.3	0.22	balance

UNCORRECTED PROOF

3. Results

3.1. Microstructure

The microstructural evolution due to thermal aging of the studied LDSS was discussed in a previous work [30]. As an example, Fig. 1 compares the microstructures of the cross section (load in SSRT was applied in the direction perpendicular to the shown section) of the as-received sample (a) and those of samples aged for 30 min at 650 °C (b) and for 5 (c) and 30 min (d) at 850 °C. In general, brief aging within the 650–850 °C range produced no evidence of χ and σ secondary phases. However, very fine chromium carbides and especially nitrides (as those indicated by blue arrows in Fig. 1) precipitated at the α/α and γ/γ grain boundaries or at α/γ interfaces. The precipitation level was augmented by rising the aging temperature and by extending the aging time from 5 to 30 min.

3.2. Slow strain rate tests performed in air

The stress − strain curves obtained with SSRT performed in air at 25 °C on LDSS 2101, both as-received and thermally aged, showed that aging of 30 or 60 min at 650 °C did not significantly influenced the mechanical behaviour of the material (not reported). On the contrary, aging at 750 °C (Fig. 2) and at 850 °C (not reported) led to an increase in alloy ductility with the increase in aging time. All the samples after SSRT in air showed a ductile type fracture. Table 2 reports the results of SSRT (in terms of ε_f %) carried out in air at 25 °C, together with HV data acquired on the cross sections. ε_f % values of the samples aged at 650 °C for 30 and 60 min were only slightly higher than that of the as-received one. Similarly, a 5 min aging at 750 °C did not modify sample ductility, while all other aging conditions at 750 and 850 °C led to a significant increase in ε_f %, more important at increasing aging temperature or time. HV values were substantially correlated with ε_f % data. In fact, increasing ε_f % corresponded to decreasing hardness values.

Table 3 reports the average values of nanoindentation hardness of both the austenite and ferrite phase, before and after the longest aging times, together with the corresponding average values of maximum contact depth (h_{max}), maximum indentation load (P_{max}) and estimated area of contact (A). In agreement with previous researchers, who carried out nanoindentation tests on ferrite and austenite in high nitrogen duplex stainless steels [22,23], the results evidence that in general the austenite phase is harder than the ferrite, due to the high nitrogen solubility and the significant strengthening effect of N interstitial atoms on the former phase. The results in Table 3 also show that, within the conditions investigated, there is a very small tendency of the ferrite hardness to increase with aging time, at the three investigated temperatures. Conversely, in comparison to as-received samples, a more significant decrease in austenite hardness is observed after 30 min at 750 and 850 °C, which appears responsible of the observed overall decrease in HV of the alloy, after these aging conditions (Table 2). The decrease in austenite hardness is likely connected to a progressive N-depletion and reduced solid solution strengthening inside the austenite grains [47], after significant precipitation of chromium nitrides at the grain boundaries [30]. The concomitant negligible increase in ferrite hardness is difficult to rationalize. In analogy with the influence of interstitial hydrogen on the ferrite and austenite hardness in duplex stainless steel [48], also nitrogen interstitial depletion, due to nitride precipitation, could induce intensification of residual stresses (typical of ferrite and austenite phases in duplex stainless steel [49–51]) and, finally, increase the ferrite hardness. The aging for 30 and 60 min at 650 °C do not significantly influence the alloy HV (Table 2) and the austenite hardness values (Table 3).

3.3. Slow strain rate tests performed in NACE TM-0177 solution

Fig. 3 reports the stress − strain curves obtained with SSRT performed in standard NACE TM-0177 solution, on both as-received and

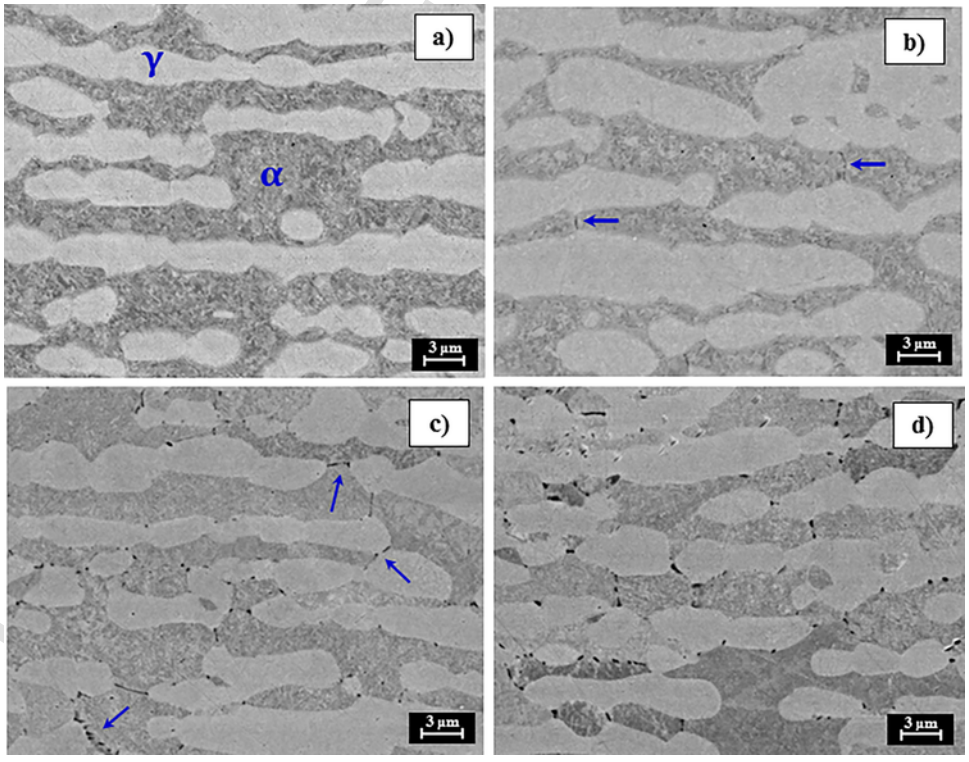

Fig. 1. BSE-SEM micrographs of cross sections of LDSS 2101 as-received (a) or aged 30 min at 650 °C (b) and 5 (c) or 30 min (d) at 850 °C. These sections are perpendicular to the load direction in SSRT.

UNCORRECTED PROOF

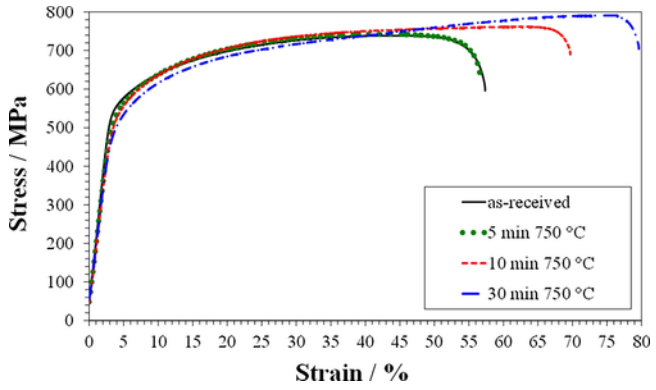

Fig. 2. Stress – strain curves obtained with SSRT performed in air at 25 °C on LDSS 2101 as-received and aged at 750 °C for 5, 10 and 30 min.

750 °C aged samples, together with the corresponding macrographs. In Table 4 the resultant ε_f % are collected. The as-received sample (Fig. 3a) evidenced a ductile type fracture with ε_f % quite similar to that obtained in air (Table 2). The samples aged for 5 and 10 min at 750 °C showed a moderate necking (Fig. 3b and c), which was accompanied by a small ε_f % reduction. A similar mechanical behaviour was noted for the samples aged at 650 and 850 °C, after exposure to the NACE solution. Instead, a definitely brittle-type fracture (without necking) was detected for LDSS 2101 aged at 750 °C for 30 min (Fig. 3d). In this case, the sample showed a significant reduction of ε_f % in comparison to air and the presence of many secondary cracks. Fig. 4 shows the BSE-SEM micrographs of the sections (parallel to load direction in SSRT) of LDSS 2101 aged for 30 min at 650, 750 and 850 °C and clearly evidence pits developed from the exposed sample surface. At 650 and 850 °C, very small cracks propagated from some of these pits, while in the sample aged 30 min at 750 °C very large cracks were documented (Fig. 4b), characterized by a mixed intergranular/transgranular propagation.

The dependence of E_{cor} vs. strain for as-received and 750 °C aged samples, collected during SSRT in NACE solution in the absence of $S_2O_3^{2-}$ is presented in Fig. 5. For the as-received sample, the E_{cor} values, starting from about -0.42 V_{SCE} gradually shifted towards more positive values and then showed fluctuations around -0.2 V_{SCE}. The sample aged at 750 °C for 10 min exhibited an initial trend similar to that of the as-received alloy, then E_{cor} set at slightly lower values (around -0.32 V_{SCE}). A significant E_{cor} shift towards more negative values (around -0.45 V_{SCE}) was measured for the sample aged at 750 °C for 30 min, the only thermal aging which produced a clearly brittle fracture during SSRT in the NACE solution. This E_{cor} value is sufficiently negative to make hydrogen ion reduction thermodynamically possible. In this environment, all other thermal aging produced E_{cor} trends characterized by nobler values, similar to those recorded for the sample aged at 750 °C for 10 min. As it will be discussed more in detail in the next paragraph, when 10^{-4} M $S_2O_3^{2-}$ was added, E_{cor} shifted in the negative direction of about 100 mV with respect to that measured in standard NACE solution and remained around -0.56 V_{SCE}.

3.4. SSRT performed in NACE TM-0177 solution in the presence of $S_2O_3^{2-}$

The presence of $S_2O_3^{2-}$ in the test solution significantly reduced the ductility of both as-received and thermally aged LDSS 2101 (Table 4). The solution with a high $S_2O_3^{2-}$ concentration (10^{-3} M) caused a very high ductility drop for all the tested samples, with no significant differences between ε_f % values. Conversely, at low $S_2O_3^{2-}$ concentration (10^{-4} M), it was possible to detect substantial differences in the ε_f % values, depending on thermal aging conditions. The macrographs of Fig. 6, acquired after SSRT performed in the standard NACE TM-0177 solution in the presence of $S_2O_3^{2-}$ at concentrations of 10^{-4} and 10^{-3} M, show a brittle-type fracture with many secondary cracks. Fig. 7a and b reports SEM images of the longitudinal section (parallel to load direction in SSRT) of the gauge length of samples as-received and aged 30 min at 650 °C, respectively, after SSRT in NACE TM-0177 solution, in the presence of 10^{-4} M $S_2O_3^{2-}$. The micrographs clearly show that the external surface of the samples is more severely corroded than those in Fig. 4 and the corrosive attack is mostly localized on the ferrite phase. Some cracks have developed with a mainly transgranular propagation, in the as-received LDSS 2101, and essentially intergranular in nature, in the sample aged 30 min at 650 °C. The longitudinal section of the samples aged 30 min at 750 (Fig. 8a) and 850 °C (Fig.

Table 2
Average values and standard deviations of ε_f % from SSRT in air at 25 °C. Average values and standard deviations of HV obtained on sample cross section.

Parameter	As received	650 °C		750 °C			850 °C		
		30 min	60 min	5 min	10 min	30 min	5 min	10 min	30 min
ε_f % air at 25 °C	57 ± 2	61 ± 3	60 ± 1	57 ± 2	70 ± 3	80 ± 2	78 ± 2	79 ± 2	83 ± 2
HV	267 ± 7	265 ± 10	265 ± 6	264 ± 6	255 ± 7	244 ± 4	244 ± 4	244 ± 3	250 ± 5

Table 3
Nanoindentation tests results (average values and standard deviations): measured parameters from the load-displacement curves (h_{max} and P_{max}), estimated area of contact calculated by Oliver and Pharr method and hardness values.

Thermal aging	phase	Maximum contact depth	Maximum indentation load	Area of contatc	Hardness values
		h_{max} (nm)	P_{max} (mN)	A ($nm^{2}*10^{+5}$)	(GPa)
as-received	ferrite	200.6 ± 2.4	5.091 ± 0.017	10.77 ± 0.24	4.73 ± 0.09
	austenite	172.24 ± 1.26	5.090 ± 0.015	8.14 ± 0.11	6.26 ± 0.10
30 min 650 °C	ferrite	197.59 ± 2.12	5.108 ± 0.016	10.47 ± 0.21	4.88 ± 0.10
	austenite	170.80 ± 1.81	5.104 ± 0.023	8.01 ± 0.15	6.37 ± 0.12
60 min 650 °C	ferrite	195.46 ± 1.41	5.120 ± 0.006	10.26 ± 0.14	4.99 ± 0.06
	austenite	172.43 ± 1.60	5.111 ± 0.015	8.15 ± 0.14	6.27 ± 0.01
30 min 750 °C	ferrite	196.63 ± 1.26	5.101 ± 0.021	10.38 ± 0.12	4.92 ± 0.04
	austenite	177.58 ± 2.09	5.101 ± 0.024	8.49 ± 0.30	5.94 ± 0.12
30 min 850 °C	ferrite	197.58 ± 0.45	5.111 ± 0.007	10.470 ± 0.044	4.88 ± 0.03
	austenite	178.21 ± 1.77	5.104 ± 0.014	8.66 ± 0.16	5.89 ± 0.12

UNCORRECTED PROOF

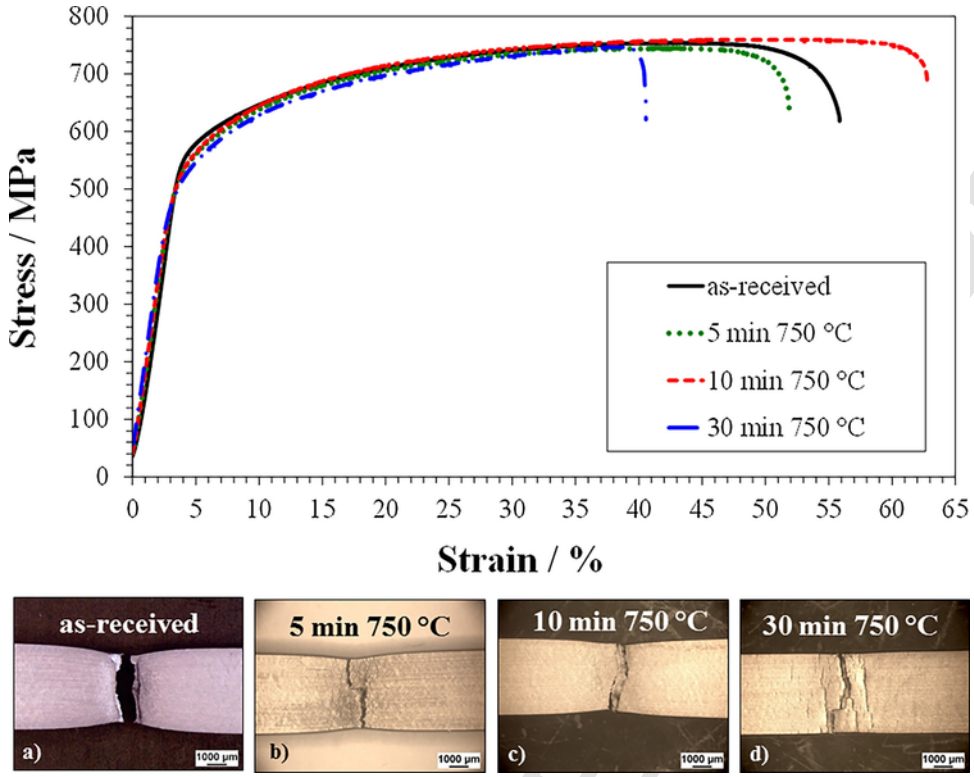

Fig. 3. Stress – strain curves obtained with SSRT performed in NACE TM-0177 solution on LDSS 2101 as-received and aged at 750 °C for 5, 10 and 30 min; below macrographs after SSRT.

Table 4
Average values and standard deviations of ε_f % from SSRT in NACE TM-0177 in the absence and presence of $S_2O_3^{2-}$ at10^{-4} and 10^{-3} M.

SSRT solution	as- received	650 °C		750 °C			850 °C		
		30 min	60 min	5 min	10 min	30 min	5 min	10 min	30 min
NACE TM-0177	56 ± 1	57 ± 1	57 ± 1	53 ± 2	63 ± 2	41 ± 2	73 ± 2	74 ± 2	77 ± 2
NACE + $S_2O_3^{2-}$ 10^{-4} M	45 ± 1	32 ± 2	33 ± 2	29 ± 2	28.0 ± 2	19 ± 2	28 ± 2	19 ± 3	20 ± 2
NACE + $S_2O_3^{2-}$ 10^{-3} M	22 ± 2			20 ± 3	18 ± 2	15 ± 2			

8b) evidences the presence of an intense surface corrosion attack mainly localized in pits and cracks, developed from the exposed surfaces. Fig. 9a and b shows that cracks of Fig. 8 have grown accompanied by a preferential attack of the ferrite phase.

Fig. 10 shows the E_{cor} vs. strain percentage trends recorded during SSRT of LDSS 2101 samples aged for 30 min at 650 and 850 °C in NACE TM-0177, in the absence and presence of 10^{-4} M $S_2O_3^{2-}$. In agreement with the trends of Fig. 5, in the presence of $S_2O_3^{2-}$, significantly more negative E_{cor} values were obtained with respect to that measured in standard NACE solution. These negative values indicate that during these tests not only hydrogen ion reduction, but also $S_2O_3^{2-}$ conversion into the more stable H_2S compound can occur [43].

3.5. SCC susceptibility in the NACE TM-0177 solution in the absence and presence of $S_2O_3^{2-}$ ions

Table 5 collects the values of R, an index used for the evaluation of SCC susceptibility. In the NACE solution, the as-received LDSS 2101 showed an R index of 0.97 with no evidence of secondary cracks. For almost all aging conditions, R values between 0.9 and 0.95 were obtained. The presence of very small secondary cracks (Fig. 4a and c), developed from pits, indicated a quite limited susceptibility to chloride-induced SCC. Instead, the sample aged at 750 °C for 30 min showed a R index significantly lower than 1, together with several secondary cracks on the gauge length (Fig. 3d), like that observable in SEM image of Fig. 4b. This behaviour evidences a high susceptibility to chloride-induced SCC. Moreover, the low E_{cor} values achieved during SSRT (Fig. 5) suggest that the contribution of hydrogen embrittlement in chloride-induced SCC cannot be excluded [52]. The addition of 10^{-4} M $S_2O_3^{2-}$ always induced R values significantly lower than 1, suggesting an important enhancement of SCC susceptibility. The effect of $S_2O_3^{2-}$was already observed for the as-received sample (R = 0.78 and secondary cracks, as reported in [40]) and the thermal aging caused a further significant decrease in R values (and in SCC resistance) as the aging temperature and generally the aging time increased. LDSS 2101 displayed the highest SCC susceptibility after 30 min at 750 °C (R = 0.23) and after 10 and 30 min at 850 °C (R = 0.24).

4. Discussion

Nanoindentation tests indicate that in as-received LDSS 2101 austenite grains are markedly harder than ferrite ones, due to solid solution strengthening by significant concentration of interstitial N atoms in the former phase.

The microstructural modifications produced in LDSS 2101 with brief aging between 650 and 850 °C are mainly connected to intergran-

UNCORRECTED PROOF

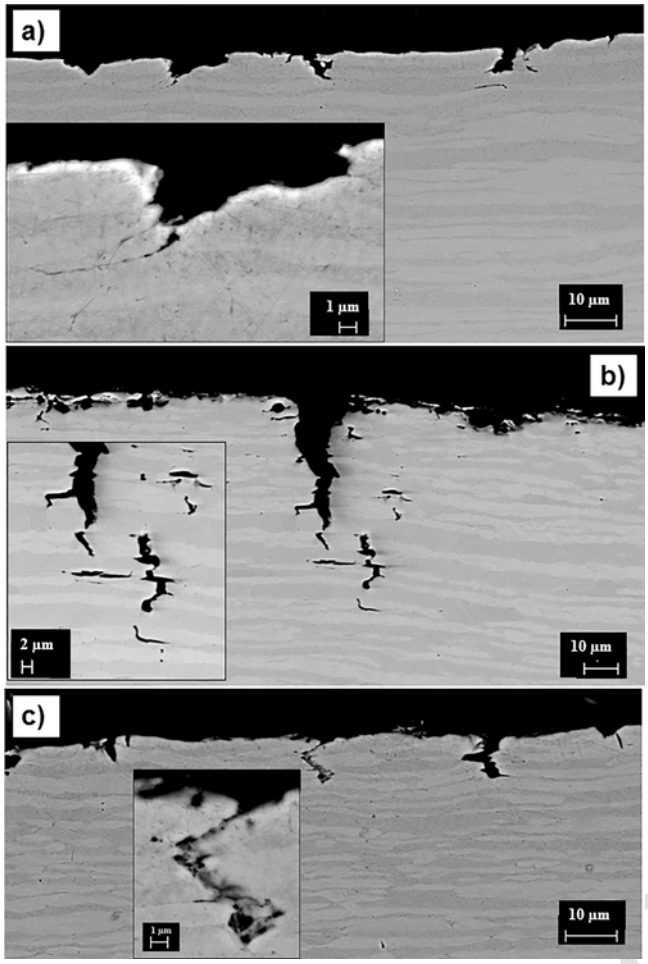

Fig. 4. BSE-SEM images of gauge length section (parallel to load direction in SSRT) of LDSS 2101 samples aged for 30 min at 650 °C (a), 750 °C (b) and 850 °C (c), after SSRT in NACE TM-0177 solution in the absence of $S_2O_3^{2-}$.

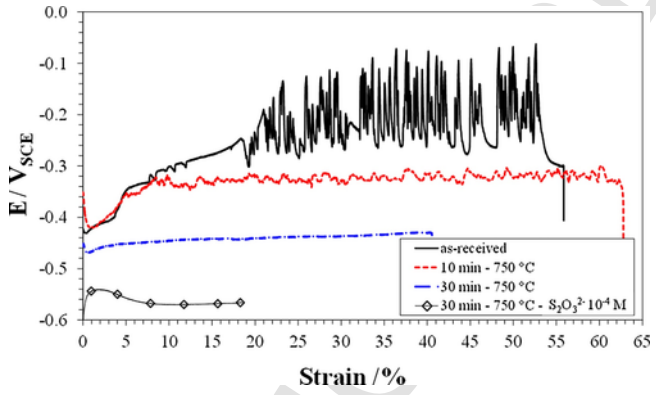

Fig. 5. E_{cor} vs. strain trends of LDSS 2101 as-received and after thermal aging (10 and 30 min at 750 °C) during SSRT in NACE TM-0177 in the absence and presence of 10^{-4} M $S_2O_3^{2-}$.

ular precipitation of chromium nitrides, which is progressively more important at rising aging temperature from 650 °C to 850 °C (e.g. Fig. 1) and increasing aging time from 5 to 30 min [30]. These conditions induce a progressive nitrogen depletion in solid solution, as suggested by the decrease in HV values and by the ductility increase in air (Table 2). Nanoindentation tests (Table 3) reveal that thermal aging determines a decrease in austenite hardness, connected to depletion in interstitial nitrogen and likely responsible of the decrease in overall alloy hardness. In ferrite, nitrogen solubility is lower and depletion of this interstitial element, reasonably less significant in this phase, is not detected by nanoindentation tests. These tests reveal instead a slight increase in ferrite hardness, perhaps due to residual stress concentration [48]. Reduced nitrogen amounts in solid solution can progressively impair passive conditions [22,53]. Tables 2 and 3 permit to deduce that particularly low nitrogen levels are achieved after aging at 750 °C for 30 min and at 850 °C.

In NACE solution not containing S2O32-, the performed thermal aging determine a higher tendency to pitting corrosion (Fig. 4), because the decreased nitrogen content in solid solution produces less stable passive conditions [54], particularly after aging at 750 and 850 °C. Thermal aging also induces local chromium depletion, particularly at temperatures lower than 850 °C, which contributes to stimulate localized attack near grain boundaries [30]. However, in general, aged LDSS 2101 shows a good resistance to chloride-induced SCC, with the exception of the samples exposed for 30 min at 750 °C (Table 5). In fact, at low temperature (650 °C) or after brief permanence at 750 °C, relatively high N levels are maintained in the alloy, capable to hinder cracks nucleation and favouring cracks repassivation [55,56]. After aging at 850 °C, only small secondary cracks are observed, since cracks repassivation is likely favoured by chromium replenishment around nitride precipitates [57]. Only after 30 min of aging at 750 °C, a high susceptibility to chloride-induced SSC is found, which could be connected to intermediate microstructural conditions characterized by both dechromized regions and rather low residual nitrogen content. After this thermal aging, a contribution to SCC from hydrogen embrittlement is also possible, as suggested by the low E_{cor} values detected during SSRT.

The SSRT carried out in NACE solution containing $S_2O_3^{2-}$ show that both as-received and thermally aged samples are sensitive to SCC. The E_{cor} values recorded during SSRT in this environment (Figs. 5 and 10 and [40]) justify the conversion of $S_2O_3^{2-}$ into reduced S-containing species, such as sulphur and H_2S [38]. This supports the hypothesis that crack propagation is connected to hydrogen embrittlement, due to surface poisoning by sulphides, which promote hydrogen penetration within the metal, ahead the crack tip [41,58]. $S_2O_3^{2-}$ reduction is catalysed by active metal surfaces and occurs preferably at pits and cracks, where also sulphur adsorption is reported to cause inhibition of the repassivation processes [43,52].

The effects of hydrogen penetration are different in austenite and ferrite. In fact, according to the literature, hydrogen diffusivity in ferrite is higher compared to that in austenite [59], even if hydrogen solubility is lower. Moreover, ferritic SS are reported to suffer from hydrogen embrittlement at lower dissolved hydrogen concentrations (i.e. $10^{-6} \div 10^{-4}$ hydrogen atoms per metal atom), in comparison to austenitic SS [60,61], suggesting that H-penetration tends to produce embrittlement preferentially in the ferrite phase. Finally, ferrite particularly if H-charged is reported to be intrinsically less corrosion resistant than austenite [60].

The results obtained indicate that, in $Cl^-/S_2O_3^{2-}$ environment, SCC susceptibility (Table 5) mainly increases with the aging time and temperature, suggesting that this phenomenon occurs more easily at decreasing interstitial dissolved nitrogen content in the alloy. Ferrite always remains the preferentially attacked phase, even if the decrease in nitrogen content impairs more significantly austenite passivity. In as-received sample and samples aged at 650 °C or at 750 °C for short times, relatively high nitrogen levels are present. Under these conditions, during SSRT the alloy undergoes a generalized corrosion attack on the ferrite phase (Fig. 7a and b), which seems to hinder cracks nucleation and growth and is likely catalysed by adsorbed sulphur [52] and stimulated by galvanic coupling with austenite. The good stability of austenite passive film could contribute to slow down SCC attack [62]. Aging at 750 °C for 30 min or at 850 °C induce a more significant nitrogen depletion in the alloy, especially in the austenite phase. These

UNCORRECTED PROOF

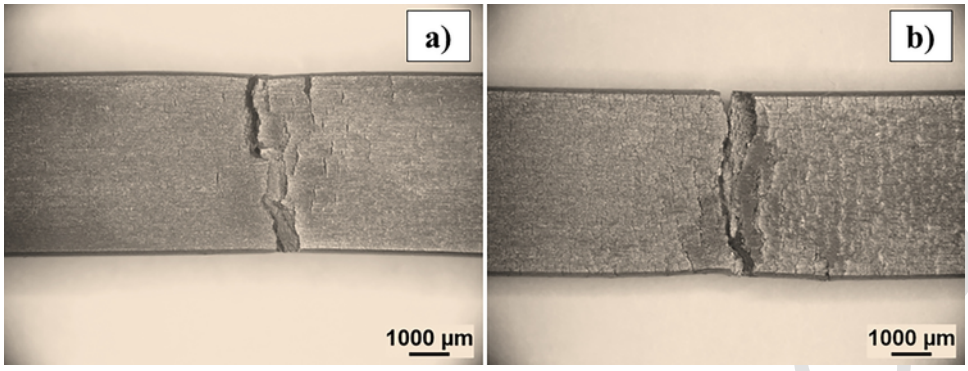

Fig. 6. Macrographs of LDSS 2101 aged 30 min at 750 °C after SSRT in NACE TM-0177 in the presence of $S_2O_3^{2-}$ at 10^{-4} (a) and 10^{-3} M (b).

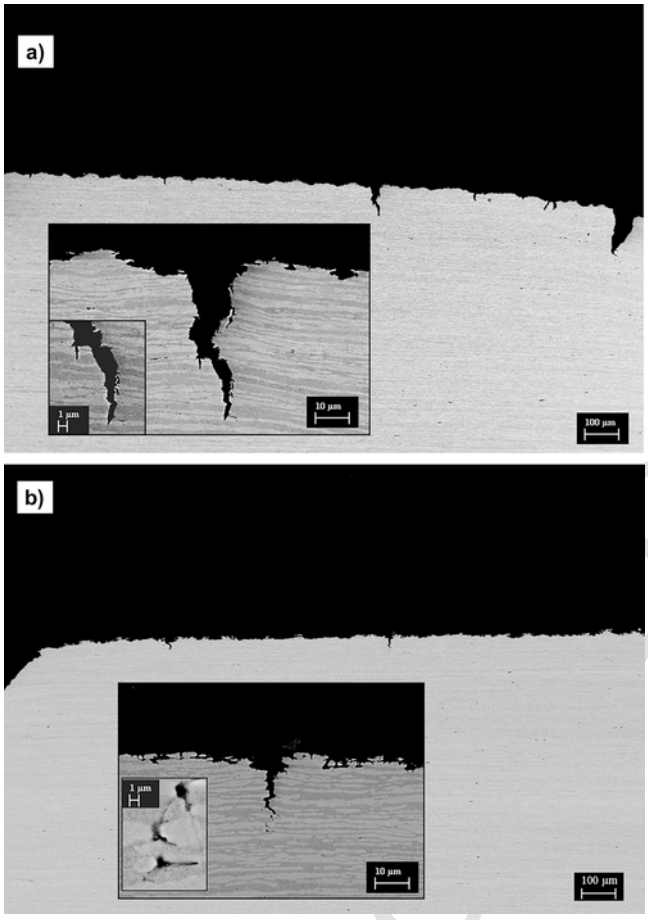

Fig. 7. BSE-SEM images of the section (parallel to load direction in SSRT) of LDSS 2101, both as-received (a) and 30 min aged at 650 °C (b), after SSRT in NACE TM-0177 solution in the presence of $S_2O_3^{2}$ at 10^{-4} M.

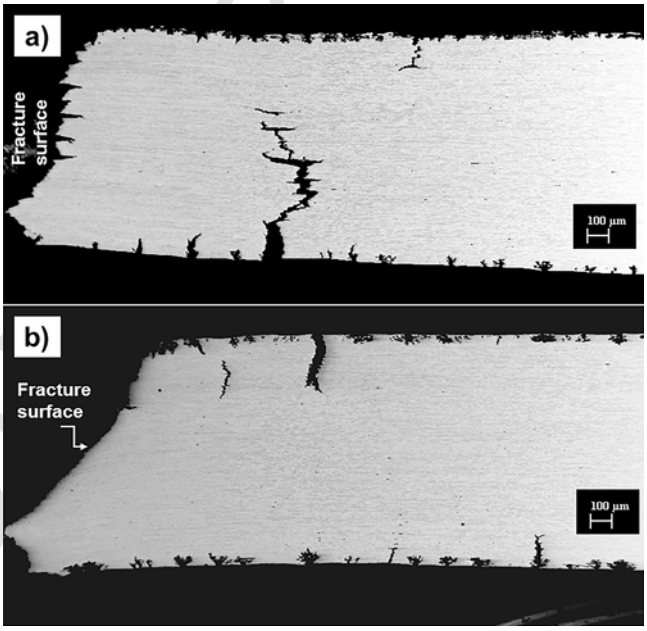

Fig. 8. BSE-SEM images of gauge length section (parallel to load direction in SSRT) of LDSS 2101 aged for 30 min at 750 °C (a) and at 850 °C (b), after SSRT in NACE TM-0177 solution in the presence of $S_2O_3^{2}$ at 10^{-4} M.

conditions favour a widespread formation of cracks and pits (Fig. 8), which exhibit preferential propagation along the ferrite paths (Fig. 9). In this case, N-depleted austenite grains can no more hinder crack nucleation and propagation, so favouring SCC susceptibility.

5. Conclusions

1. The microstructural modifications produced in LDSS 2101 with brief aging between 650 and 850 °C are mainly connected to intergranular precipitation of chromium nitrides.
2. The microstructural modifications obtained at 750 and 850 °C induce a decrease in the overall HV hardness, due to a decrease in the hardness of the austenite phase and an increase in the alloy ductility.
3. In NACE solution not containing $S_2O_3^{2-}$, only the LDSS 2101 aged at 750 °C for 30 min shows SCC susceptibility.
4. In the presence of $S_2O_3^{2-}$ in NACE solution, both as-received and thermally aged LDSS 2101 are susceptible to SCC. The resistance to the SCC gets worse at increasing aging temperature and aging time.

Acknowledgments

This work was developed within the framework of the 2007–2013 Emilia-Romagna Regional Operational Programme of the European Regional Development Fund (ERDF ROP) – priority 1 Industrial research and technological transfer: "Creation of Technopoles for industrial research and technology transfer". The material was kindly supplied by Outokumpu S.p.A.

UNCORRECTED PROOF

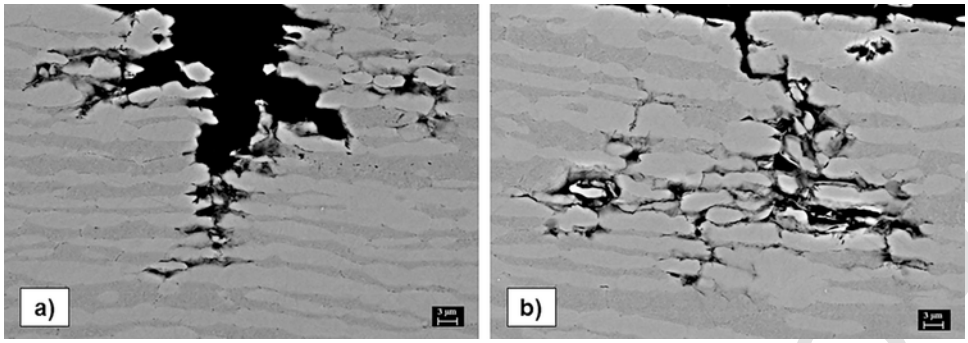

Fig. 9. BSE-SEM images of section (parallel to load direction in SSRT) of LDSS 2101 aged for 30 min at 750 °C (a) and 850 °C (b), after SSRT in NACE TM-0177 solution in the presence of $S_2O_3^{2-}$ at 10^{-4} M.

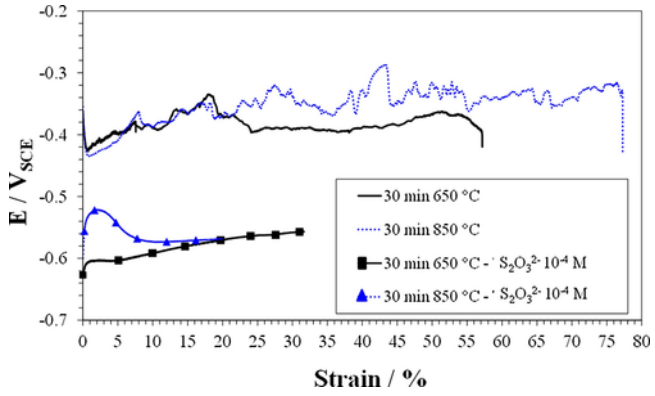

Fig. 10. E_{cor} vs. strain trends of LDSS 2101 aged for 30 min at 650 and 850 °C during SSRT in NACE TM-0177 in the absence and presence of $S_2O_3^{2-}$ at 10^{-4} M.

Table 5
SCC susceptibility index R of LDSS 2101, both as-received and thermally aged, obtained by SSRT in NACE TM-0177 in the absence and presence of $S_2O_3^{2-}$ at 10^{-4} M.

SSRT solution	as- received	650 °C		750 °C			850 °C		
		30 min	60 min	5 min	10 min	30 min	5 min	10 min	30 min
NACE TM-0177	0.97	0.94	0.95	0.92	0.90	0.51	0.94	0.93	0.93
NACE + $S_2O_3^{2-}$ 10^{-4} M	0.78	0.52	0.56	0.51	0.40	0.23	0.36	0.24	0.24

UNCORRECTED PROOF

References

[1] J. Charles, P. Chemelle, The history of duplex developments, nowadays DSS properties and duplex market future trends, In: Proc. of 8th Duplex Stainless Steels Conference, Beaune, France, 13–15 October, 2010.

[2] J. Olsson, M. Snis, Duplex –a new generation of stainless steels for desalination plants, Desalination 205 (2007) 104–113.

[3] R. Merello, F.J. Botana, J. Botella, M.V. Matres, M. Marcos, Influence of chemical composition on the pitting corrosion resistance of non-standard low-Ni high- Mn–N duplex stainless steels, Corros. Sci. 45 (2003) 909–921.

[4] B. Deng, Y. Jiang, X. Juliang, T. Sun, J. Gao, L. Zhang, W. Zhang, J. Li, Application of the modified electrochemical potentiodynamic reactivation method to detect susceptibility to intergranular corrosion of a newly developed lean duplex stainless steel LDX 2101, Corros. Sci. 52 (2010) 969–977.

[5] Z. Wei, J. Laizhu, H. Jincheng, S. Hongmei, Study of mechanical and corrosion properties of a Fe-21.4Cr-6Mn-1.5Ni-0.24N-0.6Mo duplex stainless steel, Mat. Sci. Eng. A497 (2008) 501–504.

[6] M. Pohl, O. Storz, T. Glogowski, Effect of intermetallic precipitations on the properties of duplex stainless steel, Mater. Charact. 58 (2007) 65–71.

[7] V.S. Moura, L.D. Lima, J.M. Pardal, A.Y. Kina, R.R.A. Corte, S.S.M. Tavares, Influence of microstructure on the corrosion resistance of the duplex stainless steel UNS S31803, Mat. Charact. 59 (2008) 1127–1132.

[8] N. Lopez, M. Cid, M. Puigalli, Infuence of σ-phase on mechanical properties and corrosion resistance of duplex stainless steels, Corros. Sci. 41 (1999) 1615–1631.

[9] N. Lopez, M. Cid, M. Puigalli, I. Azkarate, A. Pelayo, Application of double loop electrochemical potentiodynamic reactivation test to austenitic and duplex stainless steels, Mater. Sci. Eng. A 229 (1997) 123–128.

[10] E. Angelini, B. De Benedetti, F. Rosalbino, Microstructural evolution and localized corrosion resistance of an aged superduplex stainless steel, Corros. Sci. 46 (2004) 1351–1367.

[11] Y.H. Yang, B. Yan, J. Wang, J.L. Yin, The influence of solution treatment temperature on microstructure and corrosion behavior of high temperature ageing in 25% Cr duplex stainless steel, J. All. Comp. 509 (2011) 8870–8879.

[12] Y. Yang, B. Yan, J. Li, J. Wang, The effect of large heat input on the microstructure and corrosion behavior of simulated heat affected zone in 2205 duplex stainless steel, Corros. Sci. 53 (2011) 3756–3763.

[13] J. Hong, D. Han, H. Tan, J. Li, Y. Jiang, Evaluation of aged duplex stainless steel UNS S32750 susceptibility to intergranular corrosion by optimized double loop electrochemical potentiokinetic reactivation method, Corros. Sci. 68 (2013) 249–255.

[14] A. Elhoud, H. Ezuber, W. Deans, Influence of cold work and sigma phase on the pitting corrosion behavior of 25 chromium super duplex stainless steel in 3.5% sodium chloride solution, Mater. Corros. 61 (3) (2010) 199–204.

[15] J. Gong, Y.M. Jiang, B. Deng, J.L. Xu, J.P. Hu, J. Li, Evaluation of intergranular corrosion susceptibility of UNS S31803 duplex stainless steel with an optimized double loop electrochemical potentiokinetic reactivation method, Electrochem. Acta 55 (2010) 5077–5083.

[16] Z. Wei, J. Laizhu, H. Jincheng, S. Hongmei, Effect of ageing on precipitation and impact energy of 2101 economical duplex stainless steel, Mat. Charact. 60 (2009) 50–55.

[17] H. Liu, P. Johansson, M. Liljas, Structural evolution of LDX 2101® (EN 1.4162) during isothermal ageing at 600–850 °C, In: 6th European Stainless Steel Conference, Science and Market, Helsinki, Finland, June 10–13, 2008, pp. 555–560.

[18] E. Johansson, R. Pettersson, Lean duplex stainless steel within the oli and gas industry, vol. 4, EUROCORR 2010, Moscow, 13–17 September (2010), pp. 2869–2878.

[19] S.J. Pawel, E.E. Stansbury, C.D. Lundin, Role of nitrogen in the pitting resistance of cast duplex CF-type stainless steels, Corros 45 (1989) 125–133.

[20] I. Olefjord, L. Wegrelius, The influence of nitrogen on the passivation of stainless steels, Corros. Sci. 38 (1996) 1203–1220.

[21] J. Li, Z. Ma, X. Xiao, J. Zhao, L. Jiang, On the behaviour of nitrogen in a low-Ni high-Mn super duplex stainless steel, Mater. Des. 32 (2011) 2199–2205.

[22] C.-M. Tseng, H.-Y. Liou, W.-T. Tsai, The influence of nitrogen content on corrosion fatigue crack growth behavior of duplex stainless steel, Mater. Sci. Eng. A 344 (2003) 190–200.

[23] J. Foct, N. Akdut, Cleavage-Like fracture of austenite in duplex stainless steel, Scripta Metall. Mater. 29 (1993) 153–158.

[24] M.-H. Jang, J. Moon, T.-H. Lee, S.-J. Park, H. Nam Han, Effect of nitrogen partitioning on yield strength in nitrogen-Alloyed duplex stainless steel during annealing, Metallurg. Mater. Trans. A 45A (2014) 1653–1658.

[25] P. Kangas, J.M. Nicholls, Chloride-induced stress corrosion cracking of Duplex stainless steels. Models, test methods and experience, Mater. Corr. 46 (1995) 354–365.

[26] H. Hanninen, J. Romu, R. Ilola, J. Tervo, A. Laitinen, Effects of processing and manufactruring of high nitrogen-containing stainless steels on their mechanical, corrosion and wear properties, J. Mater. Process. Technol. 117 (2001) 424–430.

[27] M. Berner, H.P. Liu, C.O.A. Olsson, Estimating localized corrosion resistance of low alloy stainless steels: comparison of pitting potentials and critical pitting temperatures measured on lean duplex stainless steel LDX 2101 after sensitization, Corros. Eng. Sci. Technol. 43 (2008) 111–116.

[28] L. Zhang, Y. Jiang, B. Deng, W. Zhang, J. Xu, J. Li, Effect of aging on the corrosion of 2101 lean duplex stainless steel, Mat. Charact. 60 (2009) 1522–1528.

[29] J. Gao, Y. Jiang, B. Deng, W. Zhang, C. Zhong, J. Li, Investigation of selective corrosion resistance of aged lean duplex stainless steel 2101 by non-destructive electrochemical techniques, Electroch. Acta 54 (2009) 5830–5835.

[30] F. Zanotto, V. Grassi, M. Merlin, A. Balbo, F. Zucchi, Effect of brief heat treatments performed between 650 and 850 °C on corrosion behaviour of a lean duplex stainless steel, Corros. Sci. 94 (2015) 38–47.

[31] T. Zakroczymski, A. Glowacka, W. Swiatnicki, Effect of hydrogen concentrationon the embrittlement of a duplex stainless steel, Corros. Sci. 47 (2005) 1403–1414.

[32] T. Kudo, H. Tsuge, T. Moroishi, Stress corrosion cracking resistance of 22 duplex stainless steel in simulated sour environments, Corros 45 (1989) 831–838.

[33] A.A. El-Yazgi, D. Hardie, Sterss corrosion cracking of duplex and super duplex stainless steels in sour environments, Corros. Sci. 40 (1998) 909–930.

[34] F.D. de Moraes, F.L. Bastian, J.A. Ponciano, Influence of dynamic straining on hydrogen embrittlement of UNS-G41300 and UNS-S31803 steels in a low H_2S concentration environment, Corros. Sci. 47 (2005) 1325–1335.

[35] M. Sozanska, K. Kłyk-Spyra, Investigation of hydrogen induced cracking in 2205 duplex stainless steel in wet H2S environments after isothermal treatment at 675, 750 and 900 °C, Mater. Charact. 56 (2006) 399–404.

[36] Z.Y. Liu, C.F. Dong, X.G. Li, Q. Zhi, Y.F. Cheng, Stress corrosion cracking of 2205 duplex stainless steel in H_2S–CO_2 environment, J. Mater. Sci. 44 (2009) 4228–4234.

[37] S. Mukai, H. Okamoto, T. Kudo, A. Ikeda, Corrosion behavior of 25 Pct Cr duplex stainless steel in CO_2–H_2S–Cl–environments, J. Mater. Energy Syst. 5 (1983) 59–66.

[38] P.R. Rhodes, G.A. Welch, L. Abrego, Stress corrosion cracking susceptibility of duplex stainless steels in sour gas environments, J. Mater. Energy Syst. 5 (1983) 3–18.

[39] M.J. Schofield, R. Bradshaw, R.A. Cottis, Stress corrosion cracking of duplex stainless steel weldments in sour conditions, Mater. Perform. 35 (1996) 65–70.

[40] F. Zanotto, V. Grassi, A. Balbo, C. Monticelli, F. Zucchi, Stress corrosion cracking of LDX 2101® duplex stainless steel in chloride solutions in the presence of thiosulphate, Corros. Sci. 80 (2014) 205–212.

[41] S. Tsujikawa, A. Miyasaka, M. Ueda, S. Ando, T. Shibata, T. Haruna, M. Katahira, Y. Yamane, T. Aoki, T. Yamada, Alternative for evaluating sour gas resistance of low-alloy steels and corrosion-resistant alloys, Corrosion 49 (1993) 409–419.

[42] J. Tsujikawa, An alternative test method for evaluating the sour gas resistance of low-alloy steels and CRAs, Proc. Corrosion '92, Nashville, 1992, NACE Huston (1992), (paper 45).

[43] L. Choudhary, D.D. Macdonald, A. Alfantazi, Role of thiosulfate in the corrosion of steels: a review, Corrosion 71 (2015) 1147–1168.

[44] W.C. Oliver, G.M. Pharr, An improved technique for determining hardness and elastic modulus using load and displacement sensing indentation experiments, J. Mater. Res. 7 (1992) 1564–1583.

[45] 9th ed., Metals Handbook–Corrosion, vol. 13, ASM International, 1988, (p. 262).

[46] NACE Standard TM-0177-90 Standard Test Method Laboratory Testing of Metals for Resistance to Sulfide Stress Cracking in H_2S Environments, National Association of Corrosion Engineers (NACE), Houston, 1990.

[47] P. Behjati, A. Kermanpur, A. Najafizadeh, H. Samaei Baghbadorani, L.P. Karjalainen, J.-G. Jung, Y.-K. Lee, Effect of nitrogen content on grain refinement and mechanical properties of a reversion-treated Ni-free 18Cr-12 Mn austenitic stainless steel, Metallurg. Mater. Trans. A 45A (2014) 6317–6328.

[48] N. Kheradmand, R. Johnsen, J.S. Olsen, A. Barnoush, Effect of hydrogen on the hardness of different phases in super duplex stainless steel, Int. J. Hydrogen Energy 41 (2016) 704–712.

[49] S. Harjo, Y. Tomota, M. Ono, Measurements of thermal residual elastic strains in ferrite-austenite Fe-Cr-Ni alloys by neutron and X-ray diffractions, Acta Mater. 47 (1999) 353–362.

[50] M. Pohl, A. Bracke, Thermally induced microstructural changes of ferritic-austenitic stainless steels and their influence on residual stress, Z. Metallkd 90 (1999) 551–556.

[51] J. Johansson, M. Odén, X. Zeng, Evolution of the residual stress state in a duplex stainless steel during loading, Acta Mater. 47 (1999) 2669–2684.

[52] P. Marcus, J. Oudar, Corrosion Mechanism in Theory and Practice, Marcel Dekker, New York, 1995, (p. 345–346).

[53] H.-Y. Ha, C.-H. Lee, T.-H. Lee, S. Kim, Effects of nitrogen and tensile direction on stress corrosion cracking susceptibility of Ni-free feCrMnC-Based duplex stainless steels, Materials 10 (294) (2017) 1–13, https://doi.org/10.3390/ma10030294.

[54] F. Ruel, D. Tite, A. Gaugain, S. Saedlou, K. Wolski, On the depassivation mechanism of lean duplex stainless steels and influence of the partitioning of the alloying elements, Corrosion 70 (6) (2014) 636642.

[55] C.-M. Tseng, H.-Y. Liou, W.-T. Tsai, Effect of nitrogen content on the environmentally-assisted cracking susceptibility of duplex stainless steels, Metallurg. Mater. Trans. A 34A (2003) 95–103.

[56] H.-Y. Liou, R.-I. Hsieh, W.-T. Tsai, Microstructure and stress corrosion cracking in simulated heat-affected zone of duplex stainless steels, Corros. Sci. 44 (2002) 2841–2856.

[57] G.H. Aydoğdu, M.K. Aydinol, Determination of susceptibility to intergranular corrosion and electrochemical reactivation behaviour of AISI 316L type stainless steel, Corros. Sci. 48 (2006) 3565–3583.

[58] M. Gomez-Duran, D.D. Macdonald, Stress corrosion cracking of sensitized Type 304 stainless steel in thiosulphate solution. II. Dynamics of fracture, Corros. Sci. 48 (2006) 1608–1622.

[59] W.C. Luu, P.W. Liu, J.K. Wu, Hydrogen transport and degradation of a commercial duplex stainless steel, Corros. Sci. 44 (2002) 1783–1791.

[60] K. Farrel, M.B. Lewis, The hydrogen content of austenite after cathodic charging, Scripta Metall. 15 (1981) 661–664.

UNCORRECTED PROOF

[61] F. Elshawesh, J.C. Scully, Hydrogen embrittlement of 22-5 duplex stainless steel, Br. Corros. J. 33 (1998) 49–52.
[62] A.A. El-Yagzi, D. Hardie, Effect of heat treatment on susceptibility of duplex stainless steel to embrittlement by hydrogen, Mater. Sci. Technol. 16 (2000) 506–510.

UNCORRECTED PROOF